

Ultra-high sensitivity detection of bimodal probes at ultra-low noise for combined fluorescence and positron emission tomography imaging

Réjean Lebel[¶], Nikta Zarifyussefian[¶], Mathieu Letendre-Jauniaux[¶], Olivier Daigle[§], Elena Ranyuk[¶], Johannes Van Lier[¶], Brigitte Guérin[¶], Roger Lecomte[¶], Marc Massonneau[‡], Marie-Eve Ducharme[§], Yves Bérubé-Lauzière[¶]

[¶]Centre d'imagerie moléculaire de Sherbrooke (CIMS), Université de Sherbrooke, 3001 12^e ave. Nord, Sherbrooke, QC, Canada J1H 5N4; [§]NüVü camēras, 5155 avenue Decelles, Pavillon J.A. Bombardier, Montréal, QC, Canada H3T 2B1; [‡]Quidd S.A.S., Pharmaparc II Bâtiment D Voie de l'innovation. F-27100 Val de Reuil, France

ABSTRACT

Multimodal imaging is quickly becoming a standard in pre-clinical studies, and new developments have already confirmed the strength of acquiring and analyzing parallel information obtained in a single imaging session. One such application is the introduction of an internal reference moiety (e.g. radioisotope) to an activatable fluorescent probe. One of the limitations of this approach consists of working at concentrations which are within the overlapping range of sensitivities of each modality. In the case of PET/Fluorescence imaging, this range is in the order of 10^{-9} nM. Working in epi-illumination fluorescence imaging at such concentrations remains challenging. Here, we present *in vitro* and *in vivo* detection limits of a new fluorescent compound.

Keywords: Positron emission tomography (PET), Fluorescence imaging, ultra-low noise, multimodality, optical imaging, EMCCD cameras

1. INTRODUCTION

Multimodal imaging is quickly becoming a standard in pre-clinical studies, and new developments have already confirmed the strength of acquiring and analyzing parallel information obtained in a single imaging session¹. One such application is the introduction of an internal reference moiety (e.g. radioisotope) to an activatable fluorescent probe². One of the limitations of this approach consists in working at concentrations which are within the overlapping range of sensitivities of each modality. In the case of PET/Fluorescence imaging, this range is in the order of 10^{-9} nM. Working in epi-illumination fluorescence imaging at such concentrations remains challenging.

Many incentives are supporting the substitution of PET and SPECT imaging by fluorescence imaging: stability of the probes, cost of the infrastructure, risks of manipulation, and so on. On the other hand, the exquisite sensitivity of PET imaging allows for the detection of low molecular concentration targets, such as receptors. In order for fluorescence imaging to be a proper substitute, optical scanners must be optimized: highly efficient filters, powerful illumination and extremely sensitive camera.

Our center recently published several papers concerning a family of molecules named phtalocyanines (Pc) (Fig. 1), which have potential use in photodynamic therapy (PDT)³. Phtalocyanines are chelators that can trap a metal (or radiometal), which will affect their physicochemical properties. When a Zn atom is trapped, the molecule becomes highly fluorescent in water and also a very effective light sensitizer for PDT. It is also possible to insert a ⁶⁴Cu radioisotope instead, which transforms the phtalocyanine into a PET tracer⁴. This duality confers a great potential for Pc's to be used as bimodal probes, i.e. by coinjecting a mixture of both CuPc and ZnPc. While it is possible to use ⁶⁴CuPc's to track ZnPc's, it would be more useful to simply track the ZnPc directly. One of the major issues with this strategy is that some ZnPc's (e.g. ZnPcS₄) have a tendency to form aggregates *in vivo*, which reduces the fluorescence emission. Hence, to track ZnPcS₄, a highly sensitive camera is required.

Here, we characterized the limits of detection of ZnPcS₄ and compare it both with a standard commercial fluorophore (Cy7) and against the typical concentration range at which CuPcS₄ is used for PET imaging. In order to maximize the

sensitivity of our system, we use the EM N2 EMCCD camera by NüVü Cameras. This liquid nitrogen cooled camera, and its recently introduced thermoelectrically cooled version, the HNü, feature very attractive characteristics for ultra-low light and ultra-sensitive optical biomedical imaging with: the best SNR in low light applications with the same EMCCD detectors (e2v) as competitors thanks to reinvented CCD readout electronics (the CCD Controller for Counting Photons - CCCP), the lowest clock-induced charges (CIC) providing lowest background noise ($<0.001\bar{e}/\text{pixel}/\text{frame}$ with 512×512 pixels at -85°C), efficient photon counting mode to suppress the excess noise factor (ENF), high charge transfer efficiency (CTE) (up to 0.9999958) to prevent pixel leaking, high EM gain available (up to 5000), and this with no noise-filtering algorithm. Our results indicate that despite the low fluorescence of ZnPcS_4 *in vivo*, we are able to track this molecule at concentrations nearing typical CuPcS_4 concentrations, while for comparison, we show that Cy7 can be detected at concentrations one order of magnitude below typical CuPcS_4 concentrations.



Figure 1. Structure of the ZnPcS_4 , one member of the phthalocyanine family. Several different metals (M) can be chelated inside, modifying the optical properties of the Pc, or making it a radiotracer for PET imaging (e.g. ^{64}Cu).

2. METHODOLOGY

2.1 Fluorescence imaging probes

Cy7 was purchased in a Cy7 NHS ester form (GE healthcare). Properties for this molecules were taken from the website of the manufacturer (Quantum yield (ϕ): 0.28; Molar Extinction Coefficient (ϵ_{750}): $2000\ 000\text{M}^{-1}\text{cm}^{-1}$; λ_{ex} : 750 nm; λ_{em} : 767 nm). ZnPcS_4 was synthesized in-house as described previously⁵, and optical properties were found to be similar to the literature (ϕ : 10; ϵ : $250\ 000\ \text{M}^{-1}\text{cm}^{-1}$; λ_{ex} : 650 nm; λ_{em} : 676 nm) and CuPcS_4 was synthesized in-house as published elsewhere⁴. Cy7 was solubilized in dimethylsulfoxide (DMSO), dosed in methanol using its optical properties and diluted at 2 mM. ZnPcS_4 was diluted in water, dosed using UV-Vis spectroscopy using the Soret band molar extinction coefficient (ϵ : $80\ 000\ \text{M}^{-1}\text{cm}^{-1}$ at 340 nm) which is independent of solvent and aggregation, and then diluted at 2 mM in water.

2.2 Fluorescence imaging conditions

For imaging, we used the Quidd Optical Scanner (QOSTM), a planar epi-illumination optical imaging system (Quidd S.A.S., France). The illumination source (250W halogen lamp) was filtered using an extended hot mirror (NT46-386, Edmund Optics) and a dichroic bandpass filter (40 nm bandwidth centered at 655 nm for ZnPcS_4 , and 40 nm bandwidth centered at 710 nm for Cy7). Emission was filtered using both a long pass filter (695 nm for ZnPcS_4 and 720 nm for Cy7) and a dichroic bandpass filter (40 nm bandwidth centered at 716 nm for ZnPcS_4 and 46 nm bandwidth centered at 775 nm for Cy7). Dichroic filters were purchased from Semrock (Rochester, NY, USA), and the longpass filters were from Edmund Optics (Barrington, NJ, USA). The camera settings were as follows: acquisition time: 200 ms/image, EMgain of 11300, automatic background subtraction mode). Because of the high sensitivity of the camera and the location of the scanner, we observed several impacts of radioisotope emission in images. To efficiently reduce noise, the median of acquired images was used.

2.3 *In vitro* sensitivity assays

ZnPcS_4 and Cy7 were diluted to 100 nM in water inside a 96 wells plate (3:148). This solution was then diluted by 2 up to 16 times, down to a concentration of 10^{-11} (10 pM) for Cy7 and 4×10^{-10} (400 pM) for ZnPcS_4 , for a total volume per well of 100 μL . A blank (water) well was used as a control. Each dilution ladder was prepared 3 times. To minimize the variations between the location of the plates (solid angle between the wells and the camera, and between the wells and

the illumination source), we acquired the images of wells 6 at a time, and moved the plate accordingly for the wells of interest to be centered in the field of view. A set of 150 x 200 ms seconds images were acquired at each position. Image analysis was performed with Matlab. A region of interest (ROI) was drawn over the wells, and the median signal intensity of all images was calculated. Then, the median signal was averaged over the surface of each well. These results were imported in GraphPad, and one-tailed paired *t*-tests were performed to compare each dilution with the blank, until the signal was found to be non significant ($p > 0.05$). This test was selected based on the hypothesis that the signal of wells containing fluorophore contains more signal than the blank.

2.4 *In vivo* sensitivity assays

Animal experiments were conducted in accordance with the recommendations of the Canadian Council on Animal Care and of the Université de Sherbrooke Ethics Committee for Animal Experiments. Animals were kept under anesthesia (isoflurane at 1.5%). ZnPcS₄ and Cy7 were diluted in saline before injection in female nude mice (Charles River, Saint-Constant, Canada). Fluorescence imaging was performed before, during and after the injection of 100 μ L of fluorophore solution over 1 minute using an automatic injector. Images were acquired continuously every 200 ms for 10 minutes. ROIs were manually drawn over the neck, upper torso (approximately over the hearth), middle torso (approx. over the liver) and over the right back leg of the animals. The noise of the signal inside these ROIs was calculated using the root mean square deviation (RMSD) between each pixel and its 8 neighbors. The average signal (S) was also calculated, and was considered significant when $S > \text{RMSD}$. For each molecule (Cy7 and ZnPcS₄), the minimal injection dose was determined as the dose yielding significant signals for all organs.

2.5 Organ segmentation

Images acquired *in vivo* were processed using a principal component analysis (PCA) software developed in our group⁶, and based on work by Hillman and Moore⁷. Briefly, the signal as a function of time $S(t)$ in each pixel is decomposed along several vectors - the principal components, $P_1 \dots P_N$ - so that $S(t) = C_1P_1 + C_2P_2 + C_3P_3 + \dots + C_NP_N$. P vectors are selected as those most capturing the variance of the set of signals from which they originate, this variance being obtained via the eigenvalues (principal values) of the covariance matrix formed with the data. The vectors P_i , $i = 1, \dots, N$, are ordered in descending order according to their associated principal value with low order P 's containing more information - P_2 to P_4 were selected here, with C_2 , C_3 and C_4 being used respectively as the R, G and B components of a color image. The images were qualitatively graded to determine the minimal injected dose to obtain satisfying results in our experimental conditions.

3. RESULTS

3.1 *In vitro* fluorescence detection sensitivity

Dilutions of Cy7 and ZnPcS₄ were prepared and imaged using the QOSTM system endowed with the NüVü camera (Fig. 2A). The intensities in these images were analyzed using manually drawn ROIs. Results were normalized against the signal of the blank well which was set at 100 arbitrary units (a.u.) for each compound to obtain a reference value. The average intensity and standard deviations (SD) are presented in Fig. 2B. The statistically significant minimal concentrations (one tailed *t*-test) are represented as vertical dashed lines in Fig. 2B, with minimal [ZnPcS₄] (10 nM) and [Cy7] (0.6 nM) being compared with typical [CuPcS₄] (2 nM). ZnPcS₄ dilutions were performed only down to 0.4 nM since lower concentrations did not result in any signal. Note that the minimal ZnPcS₄ concentration is 5 times that of typical CuPcS₄ - but the minimal Cy7 concentration is 1/3 times the typical CuPcS₄ concentration. Given the similar quantum yield and absorption coefficients of these molecules, the aggregation of ZnPcS₄ is likely to play an important role in these results. While it is known that ZnPcS₄ is more water soluble than several other members of the ZnPc family (e.g. ZnPcS₂⁸ and ZnPcS₃C₆), it still dimerizes in aqueous media which results in a change in absorption and fluorescence⁸.

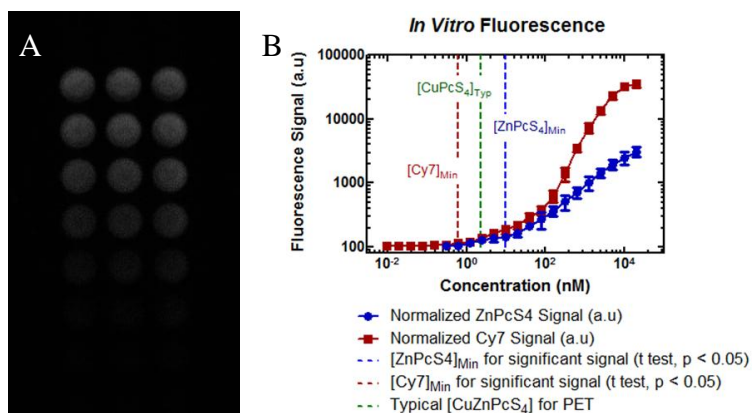


Figure 2. Fluorescence detection *in vitro*. (A) The fluorophores were successively diluted, with the ensuing dilutions placed in a 96 wells plate. (B) The fluorescence signal intensity of each concentration of fluorophore is compared with a blank. The lowest concentration at which the fluorophore produces a statistically significant signal (one tailed *t*-test, $p < 0.05$) is indicated by a dashed line.

3.2 *In vivo* fluorescence imaging

Evidence of ZnPcS4 aggregation

The preparation of injection solution allows appreciating the level of aggregation and loss of fluorescence (>95%) of ZnPcS₄ in saline (Fig. 3A, left tubes). The injection solution is compared here against the water diluted probe at identical concentration (Fig. 3A, right tubes). Despite this tremendous loss, the typical *in vivo* results using ZnPcS₄ show sufficient fluorescence for imaging (Fig. 3B). This signal is >4 times lower than that of Cy7 when injected at an identical dose (1 nmole here), which is much higher than expected from saline preparation results. Pc's are expected to bind to proteins *in vivo*, such as albumin, which likely reduces aggregation and allows for partial recovery of optical properties of the monomer molecule. Similar results were observed using micelles to de-aggregate and return PcZnS₄ to monomers⁸. Protein binding is expected to modify the biodistribution and pharmacokinetics of the probe, which would explain why more amphiphilic Pc's, such as ZnPcS₃C₆, accumulate more readily in poorly perfused tissues⁴. Note that Cy7 NHS is likely to bind covalently to proteins since it may react with available amino groups at physiological pH, which are predominantly present in proteins.

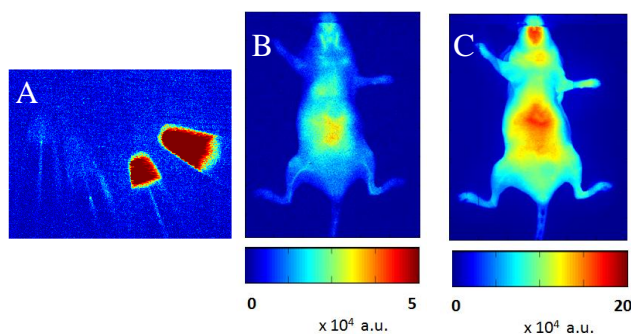


Figure 3. Atypical optical behavior of ZnPcS₄ in physiological conditions. (A) The preparation of injections in saline (the 2 tubes on the left) allowed observing a ~95% fluorescence decrease compared with water (2 tubes on the right). (B) *In vivo* fluorescence levels of ZnPcS₄ are very low, and to obtain an image with reasonable SNR after injecting 1 nmole, 300 x 200 ms images are necessary (1 min median). (C) *In vivo* fluorescence of Cy7 after the injection of 1 nmole of Cy7. This image is an average of 10 x 20 ms images (2 sec. median). Note that the *median* of the intensity, not the sum, is presented here. The greater number of images used in (B) compared to (C) does not influence the intensity level, only the noise of the image.

Determination of minimal ZnPcS₄ and Cy7 doses

Several doses of Cy7 or ZnPcS₄ were injected in nude mice, and dynamic imaging was performed during 10 minutes. At the end of the imaging session, the last 2 seconds were averaged, and SNR was determined in the form of Signal/RMSD. The SNR as a function of the injection dose is presented in Fig. 4A. Longer averaging (60 sec) resulted in increased SNR and the results are presented in Fig. 4B. Note that a difference in the aspect of the ZnPcS₄ curves is present between averaging times, which can be explained by a variation in the drawn ROI between the analyses, or time-dependent variations due to the kinetics of the molecules, which is likely to be affected by the injection dose (i.e. in the case of saturation of predilection binding sites). Results with 2 seconds integration times indicate that ZnPcS₄ detection requires a dose (4 nmol) that is ~20 times of typical CuPcS₄ doses (0.2 nmol). On the other hand, Cy7 performs much better and is visible at 0.08 nmol, well below typical CuPcS₄ doses. This indicates that ZnPcS₄ is performing poorly compared to Cy7. Note that increased integration time results in much better performance for both molecules, and optimistic extrapolation (black dotted lines in Fig. 4C) suggests that ZnPcS₄ signal could be detected at doses similar to that of CuPcS₄ for PET imaging.

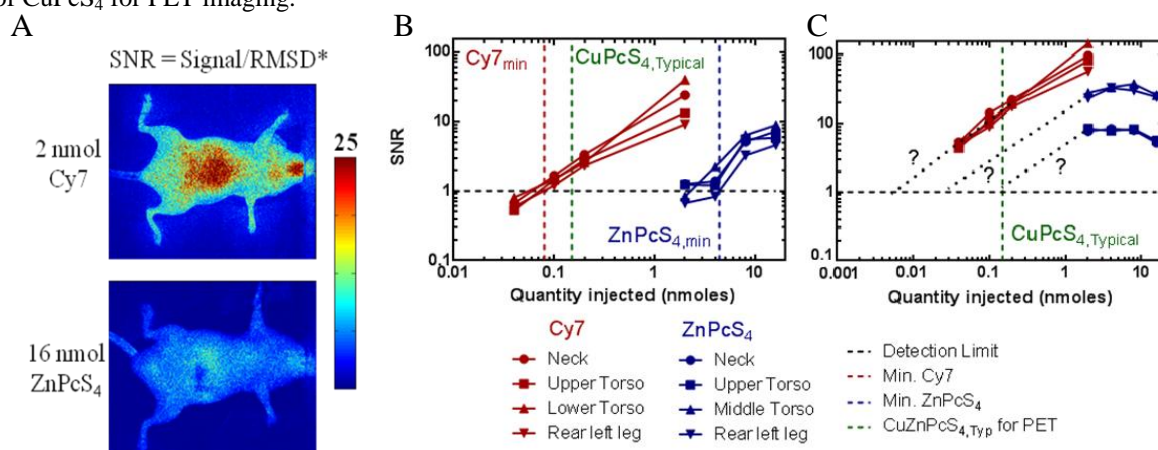


Figure 4. Fluorescence detection limits *in vivo*. (A) Typical images 10 minutes post injection of the indicated dose (10 x 200 ms integration time images). The scaling and other conditions are identical. (B) ROI SNR as a function of injection dose (10 x 200 ms integration time images). (C) ROI SNR as a function of injection dose (300 x 200 ms integration time images).

3.3 Organ segmentation based on fluorescence imaging

Using the PCA analysis described above, the organs of animals were segmented. The amphiphilic properties of Pc's are expected to lead to increased liver signal, which was selected as the organ of interest. The results of the analysis are presented in Fig. 5. The liver, located below the lungs, is visible for ZnPcS₄ down to a 2 nmol dose, while for Cy7, a dose of 0.04 nmol allows for partial liver segmentation. Note that the liver is the only organ visible for both probes at the lowest concentration; the bladder is somewhat more visible for Cy7 than ZnPcS₄, indicating that some renal elimination occurs and that part of the Cy7 did not react with proteins (which are not eliminated in the renal pathway), while very little of ZnPcS₄ is eliminated through the kidneys, as indicated by the presence of a small hotspot located in the bladder in the highest dose.

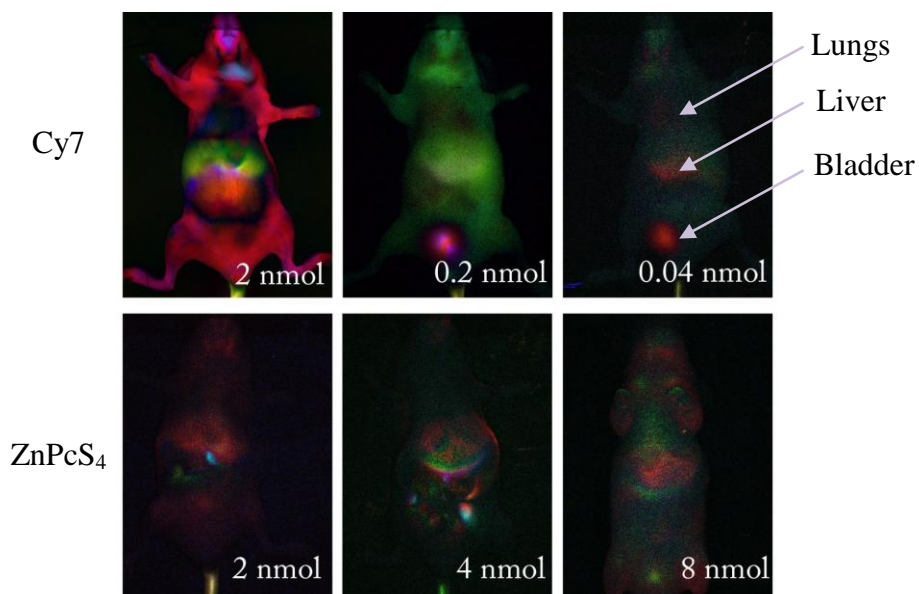


Figure 5. PCA analysis of images acquired using different ZnPcS₄ and Cy7 concentrations.

4. DISCUSSION

This work allowed determining the optical properties of ZnPcS₄ *in vitro* and *in vivo*. While our results indicate that to be detectable, ZnPcS₄ must be injected in higher doses than what is typical for CuPcS₄ PET imaging, the minimal dose for optical imaging (4.4 nmol) is well below the dose required for photodynamic therapy (100mg/kg, 2.2 μM). Hence, it would be easy to follow the ZnPcS₄ compound during PDT by optical imaging in order to optimize the irradiation by detecting at what time the tissue of interest (e.g. a tumor) reaches the maximal concentration. Obviously from our results, for more complex analysis (e.g. organ segmentation), or to track this probe in low perfusion tissues, higher concentrations of ZnPcS₄ would be required.

We observed aggregation of ZnPcS₄ in saline, and explained that it could be partially undone by protein binding. This was confirmed by an independent solubilization assay, where the fluorescence signal was improved by solubilizing Pc's in a medium containing proteins (culture medium completed with fetal bovine serum) (data not shown). We will further characterize this property in a future publication. For imaging purposes, the preparation of low aggregation ZnPcs is warranted. Our group recently submitted a manuscript presenting a set of PET/Fluorescence bimodal probes including both a ZnPc chelator bound to a second chelator, NOTA, which can be used to trap a radioactive ⁶⁴Cu. These probes were expected to have different properties, but our current results indicate that they interact even more strongly with proteins, resulting in an important fluorescence increase (data not shown). Our current results suggest that we will need to add a large hydrophilic group to our molecules (e.g. PEG) to keep them from aggregating and preserve their *in vivo* fluorescence.

Comparing Cy7 and ZnPcS₄, our results indicate that the Cy7 signal is sufficient to work at a concentration equal to that of CuPcS₄. The Cy7 solubility is not expected to be good in aqueous media⁹, but it is likely that its covalent binding to proteins will keep it from aggregating. Additionally, the Cy7 emission wavelength is located in the region of the spectrum where minimal endogenous background is present in the animals, and also where light can penetrate deeper into biological tissues. Higher signal results in higher noise: despite the fact that the background (pre-injection) fluorescence is subtracted, the noise from this signal remains. This is likely playing a role in our results, but this effect is difficult to quantify.

Using the EM N2 NüVü camera, we were able to acquire images at very high frame rates (200 ms/image). In fact, compared to the QOS Andor CCD camera (default camera), the detected signal is roughly 500 times higher. This high frame rate would potentially allow for continuous imaging while the camera is being rotated around the animal, and could potentially be used for 360° acquisitions in a fluorescence diffuse optical tomography setup.

5. CONCLUSION

In this work, we explored the limits of detectability of ZnPcS₄ *in vitro* and *in vivo* using an ultra-low noise camera (the NüVü EM N2 camera) to evaluate the feasibility of working with this molecule at similar concentrations to those typical for PET imaging with ⁶⁴CuPcS₄. Our results show that ZnPcS₄ fluorescence is likely too heavily hindered by aggregation to be used in this fashion, and we will explore other structures in the future to obtain non aggregating Pc's. On the other hand, imaging Cy7 using the NüVü camera allowed us to detect this fluorophore at concentrations (*in vitro*) and at doses (*in vivo*) much lower than typical ⁶⁴Cu PET imaging in very short (2 sec.) integration times, which is a very promising result. Longer integration times lead to even better SNR, and might allow for the detection of the fluorophore at concentrations one or more order of magnitude below PET typical concentrations.

Acknowledgements: This project has been made possible through a Technology, Exploitation and Networking (TEN) grant from the Canadian Institute for Photonics Innovation (CIPI), along with an NSERC Strategic Projects grant. Johannes Van Lier, Brigitte Guérin, Roger Lecomte, and Yves Bérubé-Lauzière are members of the FRQS-funded Centre de recherche clinique Étienne-Le Bel.

REFERENCES

- [1] E. Poulin, R. Lebel, E. Croteau *et al.*, "Conversion of arterial input functions for dual pharmacokinetic modeling using Gd-DTPA/MRI and (18) F-FDG/PET," *Magn Reson Med*, 69(3), 781-92 (2013).
- [2] C. W. Huang, Z. Li, and P. S. Conti, "Radioactive smart probe for potential corrected matrix metalloproteinase imaging," *Bioconjug Chem*, 23(11), 2159-67 (2012).
- [3] N. Cauchon, M. Nader, G. Bkaily *et al.*, "Photodynamic activity of substituted zinc trisulfophthalocyanines: role of plasma membrane damage," *Photochem Photobiol*, 82(6), 1712-20 (2006).
- [4] E. R. Ranyuk, N. Cauchon, H. Ali *et al.*, "PET imaging using ⁶⁴Cu-labeled sulfophthalocyanines: synthesis and biodistribution," *Bioorg Med Chem Lett*, 21(24), 7470-3 (2011).
- [5] H. Ali, R. Langlois, J. R. Wagner *et al.*, "Biological activities of phthalocyanines--X. Syntheses and analyses of sulfonated phthalocyanines," *Photochem Photobiol*, 47(5), 713-7 (1988).
- [6] D. Provencher, "Imagerie 3D de l'anatomie interne d'une souris par dynamique de fluorescence", Master's Thesis, Dept. of Electrical Engineering, Université de Sherbrooke, Sherbrooke (2012).
- [7] E. M. Hillman, and A. Moore, "All-optical anatomical co-registration for molecular imaging of small animals using dynamic contrast," *Nat Photonics*, 1(9), 526-530 (2007).
- [8] C. A. Laia, and S. M. Costa, "Interaction of zinc tetrasulfonated phthalocyanine with cytochrome C in water and Triton-X 100 micelles," *J Phys Chem B*, 112(14), 4276-82 (2008).
- [9] Lumiprobe, Lumiprobe product page for Cy7 NHS ester, <http://www.lumiprobe.com/p/cy7-nhs-ester> (2013) (1 February 2013).